Chapter 10 Calorimeters

10.1 Introduction

The main purpose of the LHCb calorimeters is to identify electrons and hadrons and to provide measurements of their energy and position. These measurements are required for the various trigger algorithms and for the off-line event analysis. Furthermore, the electromagnetic calorimeter should enable the reconstruction of photons and π^0 mesons. The selectivity demanded at the first level of triggering implies longitudinal segmentation of the electromagnetic shower detection. The structure chosen consists of three elements: a single-layer Preshower detector followed by a Shashlik electromagnetic calorimeter (ECAL), and a scintillating tile hadron calorimeter (HCAL).

Geometric matching of acceptance and of lateral detector segmentation facilitates the combination of the information from corresponding cells of the three detectors in the trigger processors.

The polar-angle acceptance starts at 30 mrad from the beam axis. The acceptance improvement which could be gained at smaller angles does not justify the additional cost and complications of the radiation-hard detection techniques that would be required. The outer limits of polar-angle acceptance are 300 mrad horizontally and 250 mrad vertically. The dynamic range of the readout extends up to 200 GeV in the electromagnetic calorimeter, and 300 GeV in the hadron calorimeter.

The three elements of calorimetry employ similar technologies, i.e. scintillators coupled to wavelength-shifting fibres read out by fast photodetectors. The front-end electronics will be largely unified for the whole calorimeter system.

10.2 Preshower detector

10.2.1 Performance requirements

Identification of electrons and photons at the trigger level is extremely important in LHCb. By selecting clusters exceeding an E_{T} threshold the EM single-particle trigger should provide a Level-0 rejection factor of at least 30 for minimum bias events. Good photon identification is necessary for detection of radiative B decays and for reconstructing π^0 mesons.

It was found [1] that pion rejection based on leakage into the HCAL has inherent limitations in regions of high track density: in particular the energy lost by hadrons in the HCAL near to an electron can increase the probability of mistaking the electron for a pion. As a consequence, pion rejection using only the information given by the electromagnetic and hadron calorimeters is not sufficient, and a Preshower detector is needed to provide better identification of electromagnetic particles. The transverse segmentation of the Preshower detector will match that of the ECAL. A finer subdivision will not substantially improve the detector performance, and would add considerably to its complication and cost.

A Preshower structure made of of lead and scintillator, respectively 14 mm (2.5 X_0) and 10 mm thick, has been chosen. The optimum pulse-height cut in the scintillator corresponds to 9 MIPs, yielding the performance characteristics listed in Table 10.1 [2]

Table 10.1: Single-particle Preshower performance for a cut of 9 MIPs. ε_e (ε_π) is the fraction of true electrons (pions) which pass this cut.

Energy	ε_e	ε_π	Enrichment ($\varepsilon_e/\varepsilon_\pi$)
5 GeV	0.904	0.099	9.13
10 GeV	0.975	0.073	13.36
50 GeV	0.998	0.081	12.32

10.2.2 Detector layout

The Preshower detector is located immediately upstream of the ECAL, with one-to-one correspondence between ECAL towers and Preshower cells. The Preshower is mechanically supported by the ECAL frame, the detectors being arranged in a series of drawers which can slide horizontally on rails on the left and right sides of the frame, allowing easy access to the scintillator and readout elements.

Each cell is made of a 14 mm-thick lead plate followed by a square scintillator, 10 mm thick. The tile has the same transverse dimensions as the corresponding ECAL tower. i.e. a square having 4, 8 or 16 cm sides. The scintillator will be chosen to have a high light yield and fast response. Bicron BC408 is adequate, but cheaper injection-moulded styrenic scintillators or acrylic scintillators could also be suitable. The light will be extracted from the scintillator using wavelength-shifting (WLS) fibres. This method allows the photodetectors and the readout electronics to be sited away from the beam, thus reducing the radiation dose, if necessary. Several methods are available to couple the fibres to the scintillator with good efficiency, and two possibilities are shown in Fig. 10.1:

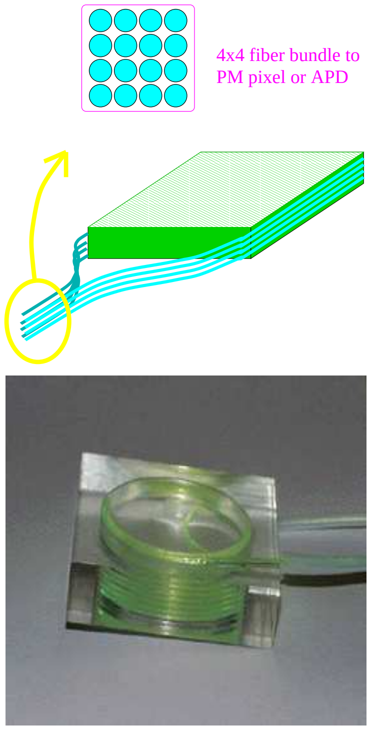

Figure 10.1: Two possible methods of coupling the scintillator tiles to the WLS fibres (see text).

Scheme (a) is similar to that employed in the hadron calorimeter and has given good results. Tests show [3] that a MIP produces more than 3 photoelectrons (p.e.) on the photomultiplier (using 1 mm diameter Kuraray WLS fibres coupled to a 1 mm BC408 scintillator plate). Scaling to 10 mm scintillator thickness, 30 p.e. will be available (the value can be almost doubled by making one end of the fibres reflecting.) In this case a bundle of 16 fibres will be directly coupled to the photodetector.

Scheme (b) is known as "spiral" coupling. A deep groove is machined inside the tile, and the WLS fibre is coiled inside it. The amount of light is similar to that measured with the first setup. The advantage is that only one fibre is used, thus simplifying the coupling to a small-area photodetector. The method is well suited to small tiles, where the total length of the coiled fibre is short and problems of transit time and attenuation are reduced.

Detailed tests will be conducted in order to study the uniformity of light response over the tile surface, and the effects on the overall detector performance.

10.2.3 Readout

The baseline solution for reading out the fibres uses multi-anode photomultiplier tubes (PMT's). The 16-pixel Hamamatsu H6568 phototube (pixel size 4×4 mm^2, pitch 4.5 mm) is well suited for coupling the 16-fibre bundle of a detector channel to a single pixel. It is compact, has low cross-talk and sufficient gain, uniformity and linearity. The readout electronics will be the same as for the calorimeters, but an ADC with only 8 bits can be used resulting in a slight cost reduction of the chain.

The electronics can be placed close to the PMT. To reduce the radiation dose the readout system (including the PMT) will be mounted on the upstream side of the radiator. If necessary, the PMT's and the electronics could be placed as far from the beam axis as necessary by making the fibres longer, with a modest reduction in light output (see Fig. 10.2).

10.2.4 Calibration

For calibration it is foreseen to use (i) a radioactive source, positioned in front of the tiles, (ii) an optical system for light injection into the tiles and (iii) a system for light injection in the PMT pixels for measuring the PMT gain. In addition the electronics chain will have (iv) a test input to be used for gain monitoring. Parts of the calibration system for the ECAL and the Preshower detector will be common.

10.2.5 APD readout option

Avalanche Photo Diodes (APD's) might become an interesting alternative to the PMT readout.

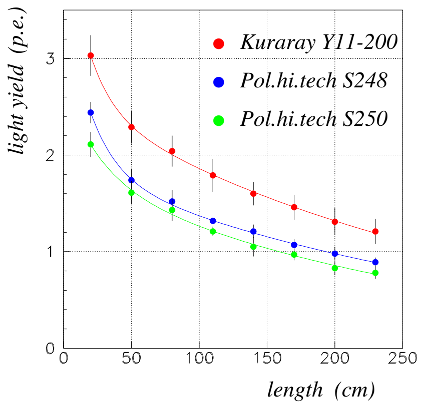

Figure 10.2: Light yield measured with different WLS fibres as a function of fibre length (1 mm BC408 scintillator).

These would have the advantage of compactness and higher quantum efficiency (Q.E.) than PMT's, and potentially could be more economical.

Manufacturers such as EG&G (Canada) and Hamamatsu commercially produce large area APD's (up to 100 mm^2), with typical gains of 50 and more. A new manufacturer (ITE, Poland) is now producing good quality APD's that have been tested successfully in a beam test.

CMS [4, 5] is executing an intensive R&D programme on APD's in collaboration with Hamamatsu to improve characteristics and to reduce costs below the $60/unit barrier, and LHCb can benefit from their experience.

For use in the Preshower, the main problem with APD's is the small light output from the tile. Taking the figures quoted above, and assuming the diode has a 60 % Q.E. in the blue region, 150 p.e. per MIP could be obtained. With a gain of 50 the signal charge would be 7500 electrons, with a detector capacitance of typically 30 – 300 pF, thus posing a serious challenge to the front-end electronics (speed vs. noise.) Therefore a larger light yield would be desirable. A collaboration with a scintillator firm (Pol.Hi.Tech) is being setup, in order to develop scintillators and/or WLS fibres with an improved matching to the APD spectral response which is peaked in the red.

10.2.6 Beam tests

First tests of a Preshower prototype using APD readout have been conducted using the X7 Test Beam in November 1997. A Preshower cell was built using a 10 mm lead radiator followed by a 10 mm thick scintillator plate (4 cm side) with "spiral" readout (see Fig. 10.1b) The 1 mm WLS fibre (Kuraray Y11) was coupled to an ITE APD. This APD had a sensitive area of 7 mm^2, a Q.E.$\approx$ 70% at 500 nm, a capacitance of 40 pF and operated at a gain of 200-400. The diode was connected to a preamplifier [6] with 11 ns peaking time. The Preshower prototype was mounted upstream of a Shashlik calorimeter module. Pulse-height spectra for 20 GeV pions and electrons are shown in Fig. 10.3 and demonstrate good separation. The efficiency for electrons over the tile surface was measured to be uniform, even in the region of the groove. The results are encouraging and more detailed tests will be conducted.

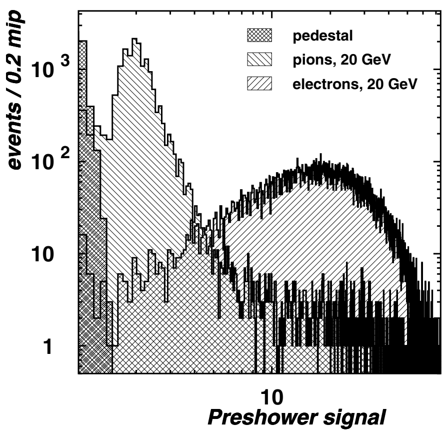

Figure 10.3: Signals from the APD Preshower prototype for 20 GeV electrons and pions.

10.3 Electromagnetic calorimeter

10.3.1 Performance requirements

The main aims of the electromagnetic calorimeter are:

- To provide electron identification at different trigger levels and at the offline reconstruction stage,
- To measure the energy of electrons and photons,
- To provide for π^0 reconstruction.

These aims define the following set of requirements for the performance of the ECAL:

Acceptance:
The z-position of the upstream face of the ECAL is 12.4 m from the interaction point. The outer dimensions are matched projectively to those of the tracking system, thus providing the polar-angle coverage of $\theta_x < 300$ mrad and $\theta_y < 250$ mrad. Due to severe radiation levels close to the beam pipe the active calorimeter volume has a central square hole of 64×64 cm^2.

Response time:
To simplify the implementation of the Level-0 trigger the signal collection time should be below 25 ns.

Transverse granularity:
The rates of photons and charged particles at the front face of the ECAL as a function of the distance from the beam pipe are shown in Fig. 10.4. The hit density varies over the calorimeter surface by two orders of magnitude. To minimize the number of readout channels the calorimeter should have a variable granularity. It is composed of inner, middle and outer regions with transverse segmentation adjusted to ensure at most a 5% charged-particle occupancy per calorimeter cell. The fine transverse segmentation is essential to improve the efficiency of π^0 reconstruction and the discrimination between electrons and charged hadrons overlapping with photons from π^0 decays.

Energy resolution:
The requirement on the energy resolution of the ECAL is rather modest. A resolution of

$$\frac{\sigma(E)}{E} = \frac{10\%}{\sqrt{E}} \oplus 1.5\%$$

(E in GeV) is sufficient to provide electron/hadron separation at a level of about 100. This energy resolution is also adequate for π^0 reconstruction. Figure. 10.5 shows the signal-to-background ratio for the π^0 signal reconstructed in minimum bias events, which is close to unity.

Radiation resistance:
The expected radiation dose strongly depends on the distance from the beam pipe, as shown in Fig. 10.6. For the innermost part of the ECAL peak doses of up to 0.4 Mrad can be reached after 1 year of LHCb operation. The longitudinal dose distribution is shown in Fig. 10.7. Since a relatively small part of the calorimeter in the vicinity of the shower maximum position suffers the maximum radiation, no significant deterioration of the performance is expected during 10 years of LHCb operation. Modules of "shashlik" calorimeter, made of injection moulded polystyrene based scintillator and Y-11 wavelength shifter (WLS) fibres, have shown only minor degradation of the energy resolution after irradiation up to 5 Mrad [7, 8, 9].

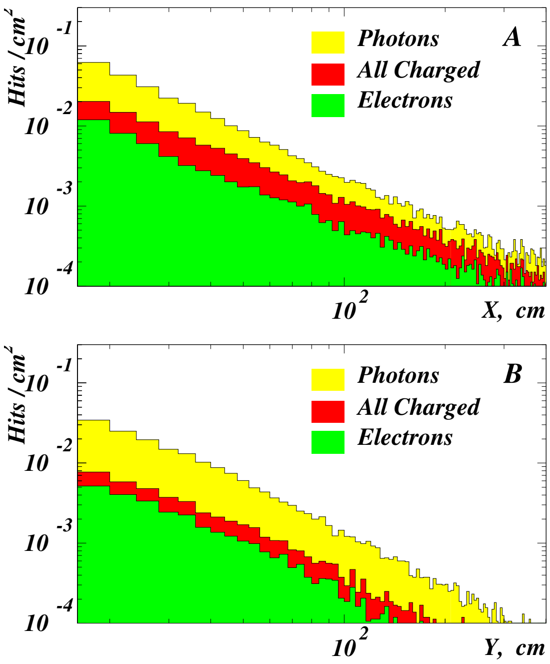

Figure 10.4: The number of particles entering the calorimeter per cm^2 per bunch crossing; (A) vs. x and (B) vs. y. Electrons and photons have energies above 1 MeV, hadrons have energies above 10 MeV.

10.3.2 Design considerations

The electromagnetic calorimeter employs the "shashlik" technology of a sampling scintillator/lead structure read out by plastic WLS fibres. This technology has been successfully developed by the HERA-B collaboration [10, 11] at DESY, the PHENIX collaboration at BNL [12] and the RD36 collaboration [13] at CERN. The combination of good energy resolution, fast response time and relatively low cost-to-performance ratio fulfil the requirements of the LHCb electromagnetic calorimeter.

The transverse view of the ECAL is shown in Fig. 10.8. The calorimeter is constructed from supermodules, shown in the figure as rectangular

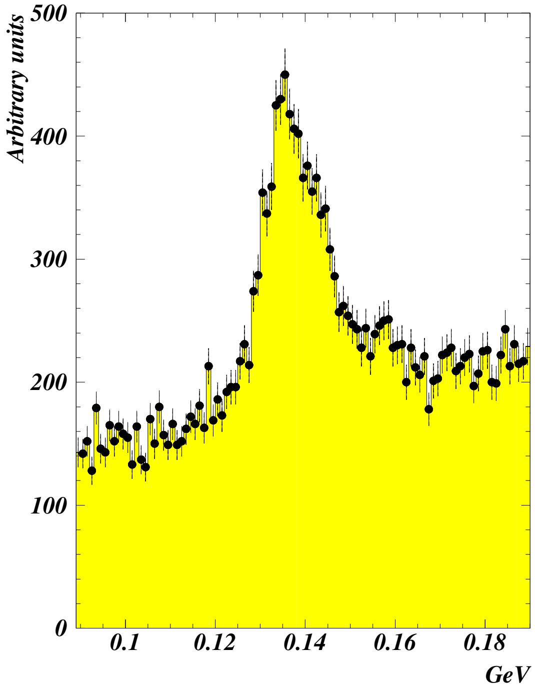

Figure 10.5: The invariant mass of two photons in minimum bias events. The minimum photon energy is 2 GeV.

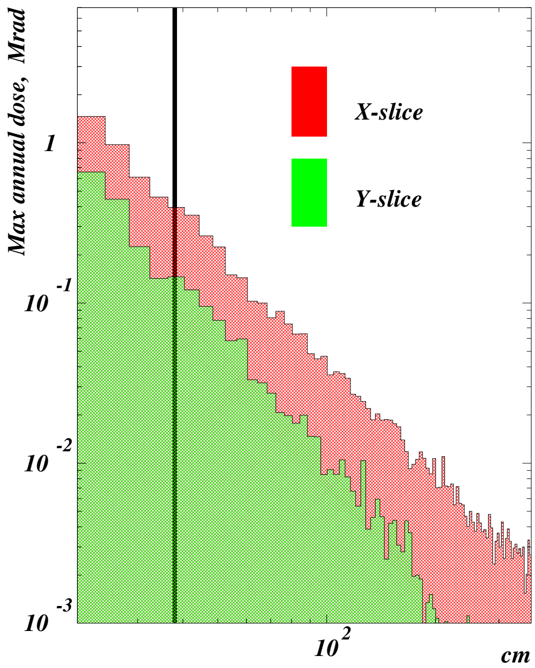

Figure 10.6: The expected annual radiation dose. The vertical line is the inner edge of the ECAL.

blocks with transverse dimensions of 64×32 cm^2. Each supermodule is a 4×2 matrix of ECAL modules which constitute the basic construction units of the calorimeter. To provide a variable transverse granularity the calorimeter is subdivided into three regions. The inner, middle and outer modules comprise 16, 4 and 1 calorimeter cell respectively. The cell parameters, as well as the number of readout channels, are listed in Table 10.2 separately for each region of the calorimeter. The supermodular geometry of the electromagnetic calorimeter facilitates its integration into the LHCb detector. The supermodules are connected mechanically at the front and backward faces and form a self-supporting structure. The structure is rigid enough to allow the left and right calorimeter halves to move sideways on rails in order to provide access for servicing. In total, there are 258 supermodules.

10.3.3 Construction features

The structure of a calorimeter module is shown in Fig. 10.9. Inner, middle and outer modules have a similar design differing by the number of calorimeter cells per module and by the WLS fibre density per scintillator tile. The module is constructed from alternating layers of 2 mm-thick lead, white reflecting paper (TYVEK) and 4 mm-thick injection moulded polystyrene-based scintillator tiles. The complete stack is compressed using stainless steel side covers, pre-tensioned and welded to front and rear steel lids. In total, there are 70 layers resulting in a total depth of 25 X_0. The transverse granularity is achieved by assembling each module layer using 16, 4 or 1 identical scintillator tiles with aluminized edges to improve light collection and prevent tile-to-tile light crosstalk. The light is read out via 1 mm diameter WLS fibres which penetrate the entire length of the module. The fibres belonging to each calorimeter cell are bundled at the end of the module and polished. A 1 mm air gap separates the surface of the WLS bundle and the phototube. The density of the fibres is a subject for optimization between light yield, uniformity of response and cost.

Readout of the scintillation light:
The operational features required from the phototubes are similar for the hadronic and electromagnetic calorimeters. The criteria governing the choice of phototube are discussed in

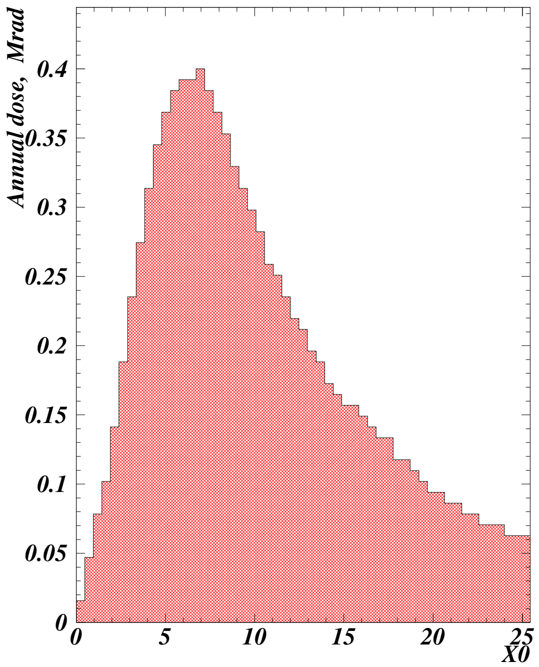

Figure 10.7: The longitudinal dose distribution for the inner region of the ECAL.

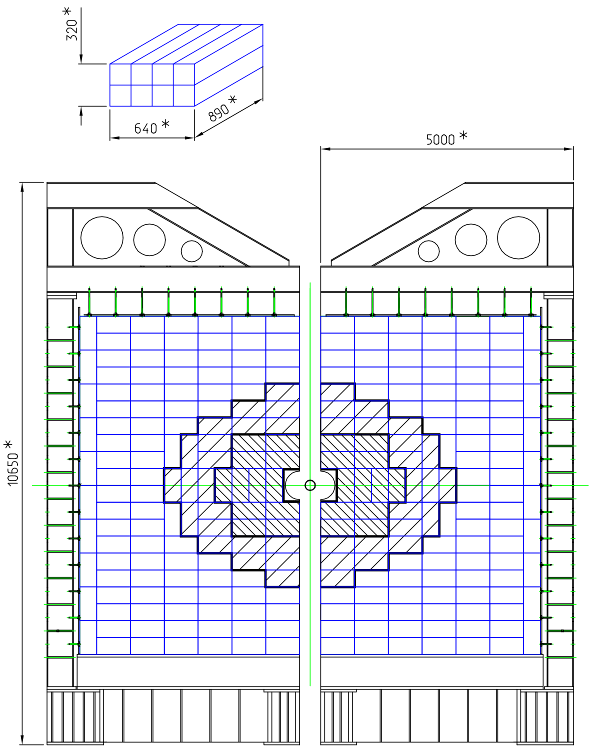

Figure 10.8: Transverse view of the ECAL. Dimensions are mm.

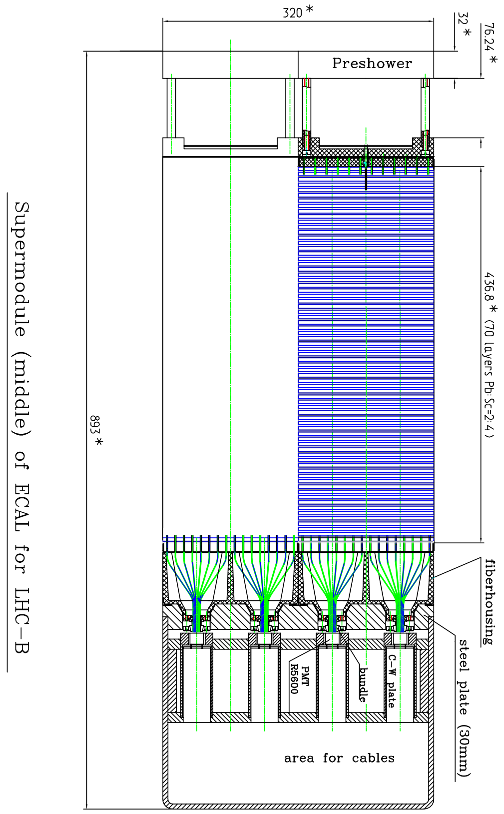

Figure 10.9: Plan view of a middle-type ECAL supermodule with its Preshower elements.

section 10.5.

10.3.4 Calibration and monitoring

In-situ calibration constants for ECAL will be obtained from experimental data using isolated particles with momenta precisely measured in the tracking system. A sufficiently large data sample ($\sim 10^3$ electrons and $\sim 10^5$ hadrons) can be collected for the calibration of each ECAL cell within a few hours of LHCb running. A complementary calibration can be performed using a sample of π^0 mesons where one of the photons converts upstream of the magnet.

The stability-monitoring system for the large number of phototubes must correct for time-dependent gain variations. Two monitoring techniques, based on the use of either multiple LED assemblies or a high intensity nitrogen laser, are under study. Monitoring systems using pulsed light sources have demonstrated better than a few percent stability. The choice will be made following further R&D.

Table 10.2: Parameters of the LHCb ECAL.

Type	Shashlik		
Absorber	Lead (2 mm plates)		
Sampling	Scintillator (4 mm plates)		
No. of layers	70		
Moliere radius	3.6 cm		
Radiation length	1.64 cm		
Depth	43.8 cm (25 X_0)		
Section	Inner	Middle	Outer
Cell size (cm)	4×4	8×8	16×16
No. of channels	3072	1344	1536
Height (cm)	320	512	832
Width (cm)	192	384	640
Weight (tonnes)	9.2	16.2	55.7
Scint. weight (kg)	1420	2486	13,442
WLS fibre type	Kuraray Y–11	BCF 91a	BCF 91a
Fibre length (km)	48.4	54.2	139.4
Photomultiplier	R5600	R5600	R5900

Table 10.3: HCAL design parameters.

Calorimeter feature	Value
Inner acceptance, ($x \times y$)	32×27 mrad
Outer acceptance, ($x \times y$)	300×250 mrad
Energy range	$0.1 \div 300$ GeV
Time resolution	< 25 ns
Shower separation	15 mrad
Radiation resistance	3 kGy/yr
Depth	$7.3\lambda_I$
Energy resolution, σ(E)/E	$0.8/\sqrt{E} \oplus 0.05$

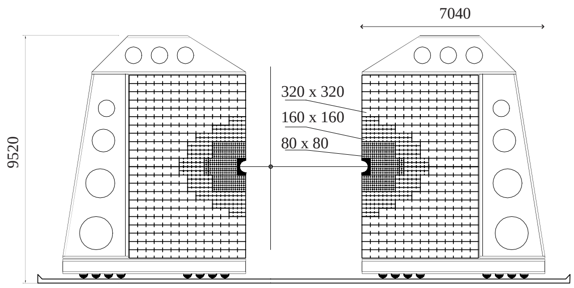

Figure 10.10: Front view of the Hadron Calorimeter.

10.4 Hadron calorimeter

10.4.1 Performance requirements

The purpose of the hadron calorimeter (HCAL) is to provide data for the trigger and to assist in background suppression when reconstructing B decays.

At the trigger level the HCAL must:

- provide a single-particle transverse-energy measurement of high p_{T} hadrons,
- improve electron and hadron separation especially for high-energy particles.

In addition, at the reconstruction stage, the HCAL will improve electron and muon identification.

The performance parameters expected from the HCAL design are summarized in Table 10.3.

10.4.2 HCAL design

A schematic view of the HCAL is shown in Fig. 10.10.

Like the ECAL it consists of three regions with different granularity. The lateral cell segmentation has to satisfy the following criteria:

- it must measure the shower position, with a small contribution to the p_{T} measurement error of a single hadron,
- it must allow good two-hadron spatial separation,
- The number of channels should be kept low to minimize the cost.

A four to one correspondence in the segmentation between the HCAL and ECAL will be maintained throughout the detector. Hence the cell sizes range from 8×8 cm^2 at the centre, through 16×16, to 32×32 cm^2 at the periphery.

The technology consists of a scintillator/iron sampling structure with the scintillating tiles parallel to the beam axis and with passive radiator made of steel plates. The overall dimensions of the active surface are 8.96 m $\times$ 7.04 m. The beam pipe passes through a 0.64 m $\times$ 0.64 m square hole at the centre. Shielding material is placed between the beam pipe and the inner edge of the HCAL.

The scintillation light is transferred by the WLS fibres to the rear of the calorimeter where it is detected by photo-multipliers. This technology, already tested in the ATLAS TileCal [14] design, has several advantages:

- the calorimeter has the 'natural' depth of passive material between tiles, of the order λ_{I} along the direction of the hadron shower development,
- in the transverse direction, the spacing be-

tween tiles is of the order of one radiation length, X_0, suitable for electromagnetic cascade development,

- the fibres have a large contact surface with the tiles providing efficient light collection,
- the scintillator is produced by injection-moulding techniques and is cheap,
- the detector can be segmented both transversally and longitudinally,
- the detector is easily assembled and has good mechanical properties.

The design parameters of the Hadron Calorimeter are summarized in Table 10.4.

Table 10.4: Hadron Calorimeter: summary of features.

Active area m^2	8.96×7.04
Average thickness	$68\ X_0$, $7.3\ \lambda_I$
Cell size, cm^3	$8 \times 8 \times 153$
	$16 \times 16 \times 153$
	$32 \times 32 \times 137$
Sampling structure	6 mm steel plate
	4 mm steel spacer
	3 mm scintillator
Total weight, tonnes	597
Segmentation	2-fold in depth
Number of cells:	
— with 8×8 cm^2	512 cells
— with 16×16 cm^2	336 cells
— with 32×32 cm^2	736 cells
Total number of channels	3144
Photomultiplier	R5900 Hamamatsu

10.4.3 Calibration and monitoring

The hadron calorimeter is required to supply data for the Level-0 trigger. Its stability and performance must therefore be continuously checked and maintained. Three different types of calibration are foreseen:

- a ^{137}Cs radioactive source is driven hydraulically inside the calorimeter through a 8 mm diameter stainless steel tube,
- LED/laser pulses monitor the stability of the PMT-electronics chain,
- test-charge injection calibrates the ADC's and checks the stability of the trigger logic.

The calibration system has to maintain the overall stability of the calorimeter response within a tolerance of a few percent, compatible with the resolution of the detector at the high end of the energy range. The principles of design and performance of the calibration system were tested during the prototype construction and in beam tests. They are described in the following section.

10.4.4 Prototype beam test

During 1997, three prototype modules of dimensions $16(H)\times 96(W)\times 153(D)$ cm^3 were constructed and tested. The scintillating tiles, made of PSM 115 with 1.5% PTP and 0.015% POPOP were injection moulded. The Pol.Hi.Tech. type S250 WLS fibres, aluminised at the upstream end, were glued in bundles and polished to an optical finish on the rear side of the module.

All tiles had dimensions $157 \times 156 \times 3$ mm^3 and were wrapped in a TYVEK envelope, the WLS fibres running between scintillator and TYVEK on both sides of the tiles. Measurements of tile samples using a β-source show uniformity of the light response within 5% (Fig. 10.11).

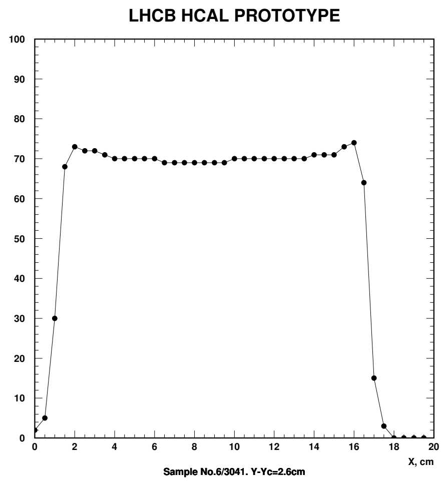

Figure 10.11: The typical tile response (pulse height, in arbitrary units) to a $\beta-$source scanned between the two readout fibres.

The prototype detector contained a 8 mm diameter stainless steel pipe through which a ^{137}Cs radioactive source could be hydraulically driven (Fig. 10.12).

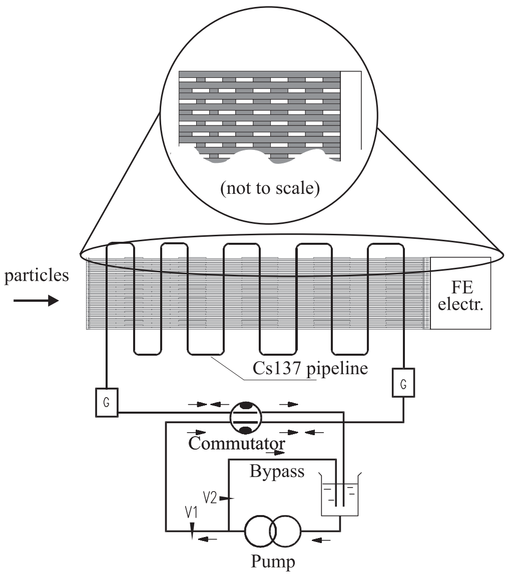

Figure 10.12: The schematic view of the HCAL calibration system. The zoom illustrates the scintillators in the tile array with the vertical scale magnified 10x compared to the horizontal.

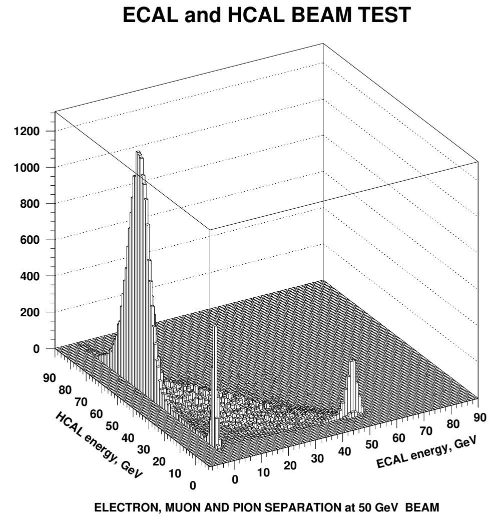

Figure 10.13: Combined beam test of ECAL and HCAL. Muons, electrons and pions are clearly separated.

Using FEU84 PMT's, with a quantum efficiency of 12-15%, a yield of 30-50 photoelectrons/GeV was obtained. Tests of the prototype response at different energies show good agreement compared to Monte-Carlo predictions using a GEANT simulation of hadronic showers. Data were taken with a Shashlik ECAL module placed upstream of the HCAL. The scatter plot shown in Fig. 10.13 illustrates the combined ECAL and HCAL performance in separating electrons hadrons and muons.

10.5 Photodetectors and front-end electronics

The Preshower, ECAL and HCAL detectors generate fast secondary light signals by the conversion in wavelength-shifting fibres of the primary scintillation of plastic plates. The signals from these detector elements will be digitised and channeled to the data acquisition system according to the general LHCb front-end electronics standards. They will also be transmitted to the Level-0 trigger hardware. The main difference between the three systems is their light yield. Common solutions for detector readout will therefore be promoted, hopefully leading to cost-effective construction and simpler operation.

10.5.1 Phototubes:

The list of requirements for the photomultipliers is given in Table 10.5. The light yield in the ECAL cells will be in excess of 1000 photoelectrons per GeV. The mean anode current has been chosen small enough (5 μA) to ensure a gain degradation of less than 10% per year of operation. WLS fibres incorporating the K27 dye emit a light spectrum peaked at 490 nm. Phototubes with green-extended photocathodes are therefore preferred.

The same requirements apply to the HCAL, but the light yield will be of the order of 50 photoelectrons per GeV. The 0.1-300 GeV dynamic range will be covered by operating the phototubes at a higher gain.

The Hamamatsu R5600 and 5900 series meet these requirements. They are compact, have good timing properties, high limits on mean anode current and good linearity.

Uniformity of the calorimeter response requires the photocathode to be uniform over the area coupled to the fibres or, if this is inadequate, the use of a light mixer in front of the PMT window.

The high voltage supply has to provide for stable PMT operation at high particle rates up to 10

Table 10.5: Requirements for the ECAL phototubes.

	Inner section	Middle section	Outer section
E_e max	200 GeV	100 GeV	50 GeV
$<E>$ max/bx	0.12GeV	0.015GeV	0.024GeV
Light yld./GeV	1200 p.e.	1200 p.e.	4500 p.e.
$<I_A>$	$\leq 5\mu A$	$\leq 5\mu A$	$\leq 5\mu A$
I_A max	10 mA	27 mA	10 mA
gain	$\leq 5*10^3$	$\leq 4*10^4$	$\leq 7*10^3$

MHz. A Cockroft-Walton base can provide an average output current as large as 0.1 mA and current pulse amplitude up to 200 mA. Several thousand channels of such a system have been built and tested for the HERA-B calorimeter.

10.5.2 Front-end electronics

Design requirements:
Taking into account the performance requirements for the energy resolution of the calorimeters, a single design with a limited dynamic range is foreseen. The following conditions should be satisfied :

- Shaping within 25 ns to avoid pile up between consecutive bunch crossings. The noise should be smaller than the digitisation error,
- Stable pedestal,
- 12-bit dynamic range. In the ECAL, the energy range covered will vary with the polar angle:
  - 50 MeV → 200 GeV for the inner region
  - 25 MeV → 100 GeV for the middle region
  - 12.5 MeV → 50 GeV for the outer region

  No B-physics is lost at the high-energy scale (there are almost no B events with e^-, γ, π° above an E_T of 10 GeV/c). At the low-energy end the binning error of ± 1.3 digits, which is obtained after pedestal subtraction and clusterisation, will remain negligible compared to the detector energy resolution at 4 GeV, 2 GeV and 1 GeV, respectively in the 3 calorimeter regions,
- Digitisation of the events at 40 MHz and their storage in a 128-deep pipeline buffer providing 3.2 μs latency,
- An 8-bit transverse-energy measurement must be supplied to the Level-0 trigger logic.

Analogue signal shaping:
Various solutions are being studied for the amplifier shaper: a 5-fold 2.6 nsec integration (Gaussian shaping), or delay-line-clipped integrator. Both unipolar and bipolar versions are under study. The final choice will result from a compromise between critical timing (better for the unipolar delay-line-clipped integrator) and baseline shift at high rate (better for the bipolar Gaussian shaper).

A delay-line-clipped shaping electronics schematic, which incorporates a slow integrator for calibration and monitoring purposes is displayed in Fig. 10.14. This circuit generates a flat-topped ouput pulse which is robust against jitter.

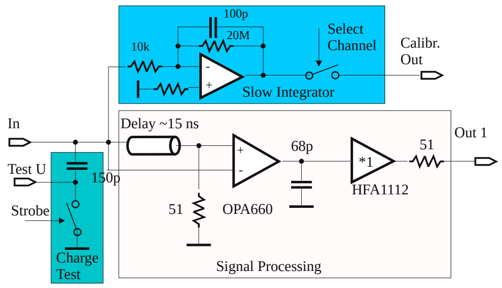

Figure 10.14: Block diagram of delay-line-clipped shaping electronics.

A custom designed implementation of front-end electronics:
The system consists of front-end cards serving 16 channels (Fig. 10.15) and controller cards used to read out 8 front-end cards. The front-end cards contain, for each channel, an amplifier-shaper, a 12-bit 40 MHz ADC with adjustable strobe timing, a register to resynchronize the ADC's output, a 4 K memory used as a look-up table to correct the pedestal, the gain, and possible nonlinearity. A second memory is used to convert the ADC signal to E_T values, as required for the Level-0 trigger. The memory is followed by a FIFO pipeline, 128 deep, which is used to store the signal for a latency of 3.2 μs. After the Level-0 strobe, data are buffered and sent by a 48 line bus to a controller card.

The amplifier-shaper would be built as an ASIC for 4 channels. The remaining electronics use commercial components. For example, the memories are presently available as 8-bit 8K 40 MHz memories, the pipelines as 18-bit 256-cell FIFO's shared

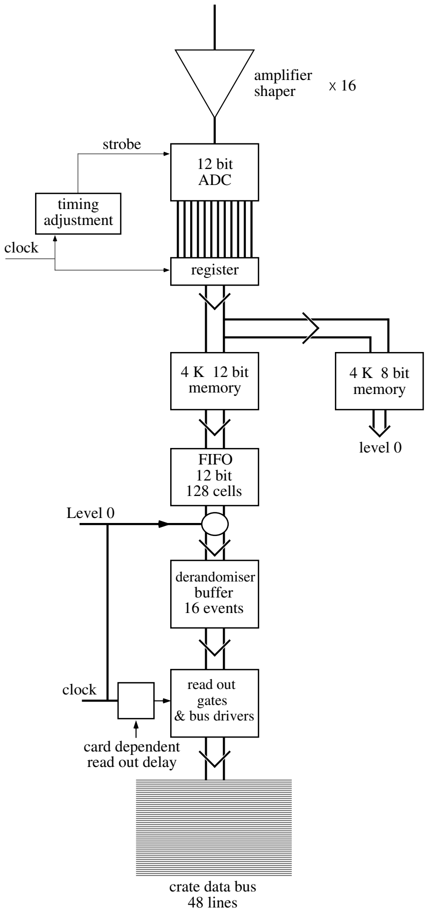

Figure 10.15: Schematics of a custom designed front-end electronics chain.

between channels. The buffer and gate readout would be implemented as one FPGA for 4 channels.

The readout card receives the data from 8 front-end cards, transferred by multiplexing in 32 steps after a Level-0 trigger. Channel address, bunch ID and event ID information are added at this stage (24 bits). It is followed by a 128-event buffer (which could be implemented as 4×4 K 18 bit commercial FIFO). Following a Level-1 trigger, data would be zero suppressed and sent by a high speed link to the DAQ. A single card in a crate can host two controllers, each serving 8 readout cards (see Fig. 10.16).

An implementation based on the FERMI system: A solution considered for signal digitization and processing is the digital FERMI system [15], suitably adapted to LHCb requirements. Initially designed for high precision calorimetry it is im-

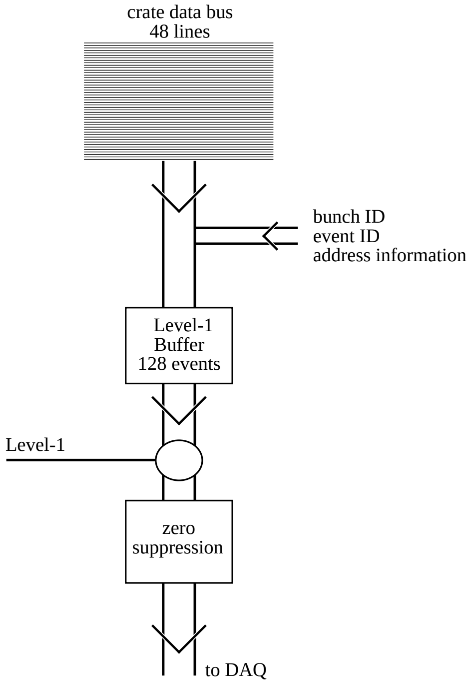

Figure 10.16: Readout card; functional scheme.

plemented as a silicon-on-silicon multichip microsystem with a variety of functional components located on large Si substrates ($\sim 5 \times 5$ cm^2) with 4 metal layers.

It could incorporate ADC, pipeline delay (Level-0 and Level-1 buffers), trigger data extraction and service ASIC's.

A number of FERMI microsystems can be mounted on a board, with external circuitry providing the following functions:

- combine data from several FERMI's into one trigger-cell value which is transmitted to the global Level-0 trigger processor,
- generate addresses at each clock signal, pointing at free storage locations for the sampled input data and to generate the pointers required for readout,
- transfer data to the external front-end driver units,
- initialize, control and supervise the FERMI's.

Figure. 10.17 displays the general organisation of this electronics chain.

The choice between the various possible electronics designs will be made after thorough assessment of their performance and costs.

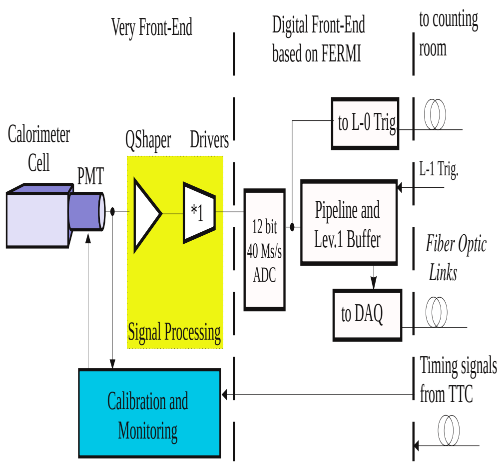

Figure 10.17: Schematic of the calorimeter electronics chain using the FERMI system.

Location of electronics:
All front-end electronics associated to the calorimeters will be housed in crates, close to the detectors. Cable lengths between PMT and electronics will be 6-8 m and the crates can be located where the annual radiation dose should not exceed a few hundred rads, allowing the use of standard components.

References

[1] S. Conetti, I. Korolko and G.Wilkinson, "Performance of the LHCb Calorimeter Triggers", LHCB/98-014.

[2] M. Adinolfi, "Optimization of the LHCb Preshower", LHCB/98-015.

[3] M. Adinolfi et al., "Readout optimization for the KLOE QCAL tile calorimeters" - Proc. 7th Pisa Meeting on Advanced Detectors (1997). La Biodola (1997).

[4] CMS Collaboration, "CMS Technical Proposal", CERN/LHCC 94-38 (1994).

[5] A. Karar et al., "Investigation of Avalanche Photodiodes for EM Calorimeter at LHC", CMS-TN/95-095 (1995).

[6] P. Aspell et al., (RD36 Collaboration), Nucl. Instr. and Meth. in Phys. Res. A 376, 17 (1996).

[7] SDC Collaboration, "SDC Technical Design Report", SDC-92-201, SSCL-SR-1215 (1992).

[8] V.G. Vasil'chenko, "New results on plastic scintillators radiation damage", CMS TN 94-220 (1994).

[9] E. Tarkovsky, "The HERA-B electromagnetic calorimeter", NIM A379 (1996) 515-517.

[10] HERA-B Collaboration, HERA-B Proposal, DESY-PRC 94/02 May 1994.

[11] HERA-B Collaboration, HERA-B Design Report, DESY-PRC 95/01 January 1995

[12] Bazilevsky A. et al., IEEE Transactions on Nuclear Science v.43, No. 3 (1996).

[13] J. Badier et al., "Shashlik Calorimeter: Beam Test Results", NIM A348 (1994) 74-86.

[14] ATLAS - Tile Calorimeter TDR, CERN/LHCC 96-42.

[15] B. Lofstedt et al., "FERMI: A digital Front End and Readout MIcrosystem for High Resolution Calorimetry", Proc. Second workshop on electronics for LHC experiments, Balaton, 23-27 Sep. 1996, (1996) 84.